

Closed-Form Expressions for the Correlation Coefficient of Directive Antennas Impinged by a Multimodal Truncated Laplacian PAS

Laurent Schumacher, *Member, IEEE*, and Balaji Raghoehtaman, *Member, IEEE*

Abstract—This paper addresses the derivation of a closed-form expression for the correlation coefficient of a pair of antenna elements at the base station. The closed-form expression is derived for the case of a multimodal truncated Laplacian power azimuth spectrum that impinges on antenna elements exhibiting a directive radiation pattern that is widely used in standardization bodies. To avoid numerical instability, an approximation for small azimuth spreads is presented. The proposed closed-form expression, along with its approximation, is successfully validated against the numerical computation of the correlation coefficient.

Index Terms—Antenna radiation patterns, correlation, MIMO systems.

I. INTRODUCTION

THE correlation between the waves impinging on two antenna elements has been widely studied both experimentally and mathematically [3]–[10]. It has been shown that the evolution of the correlation coefficient as a function of the normalized distance between the antenna elements mostly depends on the power azimuth spectrum (PAS) and on the radiation pattern of the antenna elements.

Measurement results are presented in [3] and [4] along with additional references. Complementarily, in a more analytical perspective, the seminal work of Lee [5] modeled the PAS in outdoor scenarios as the n th power of a cosine function. This model has however been regarded as inconvenient since it does not enable one to derive closed-form expressions for correlation coefficients [6]. Hence, two other distributions, a truncated Gaussian and a uniform one, have been introduced in [3] and [7], respectively. More recently, a truncated Laplacian distribution has been proposed in [8] as the best fit for outdoor measurement results in urban and rural areas. For these three distributions, namely uniform, truncated Gaussian, and truncated Laplacian, the correlation coefficient has been computed as a function of the normalized distance using the angle of incidence and the azimuth spread (AS)¹ as indexing variables. Results for both uniform and truncated Gaussian PASs are presented in [6]. Additional results for the uniform distribution

are available in [9] and [10]. Results for the truncated Laplacian distribution have been presented in [8].

It can be noted that all the analytical results cited above do not include any kind of directive antenna pattern. The inclusion of such antenna patterns gives a more complete and useful description of the correlation coefficients. In this paper, we use one of the most widely used antenna patterns. It is used for sectorized antennas in cellular systems. It has been used in several standardization bodies, including 3GPP and 3GPP2, for the evaluation of system performance in the past [1]. It will also be used in similar evaluations with respect to multiple antenna technology in the future [2].

Additionally, it has been observed in [11] that the radio waves could gather in several clusters distributed over the space domain. A model of this clustered propagation, also called multimodal in [12], was introduced in [13] as an extension to the space domain of a similar clustered model originally introduced in the time domain for indoor environments [14]. However, due to the fact that the model [13] defines the mean angle of incidence of the spatial clusters as a random variable uniformly distributed over $[0, 2\pi]$, it can hardly be used to characterize the properties of a given scenario. This paper will therefore address multimodal Laplacian PAS where the mean angle of incidence is regarded as a deterministic parameter instead of a stochastic one.

In Section II, the analytical expressions for the antenna radiation pattern and the truncated multimodal Laplacian PAS are introduced. Then the closed-form expression for the correlation coefficient is derived in Section III. It appears that its computation is numerically unstable for small ASs. Hence, a suited approximation is presented in Section IV. In Section V, the closed-form expression, including its approximation for small ASs, is validated against the outcome of numerical integration in the case of isotropic and directive radiation patterns on one hand and for mono- and bimodal power azimuth spectra on the other. Finally, some conclusions are presented in Section VI.

II. RADIATION PATTERN AND PDF OF ANGULAR SPREAD

A. Antenna Radiation Pattern

The gain in decibel of a directive antenna in azimuth ϕ is given by the radiation pattern $G_{\text{dB}}(\phi)$. In the case of the base station in a cellular system, one of the widely used radiation patterns is defined as [2]

$$G_{\text{dB}}(\phi) = \max \left[-\alpha \left(\frac{\phi}{\phi_{3 \text{ dB}}} \right)^2, -\beta_{\text{dB}} \right] \quad (1)$$

Manuscript received May 23, 2003; revised March 9, 2004; accepted June 4, 2004. The editor coordinating the review of this paper and approving it for publication is C. Xiao.

L. Schumacher is with the Computer Science Institute, FUNDP-The University of Namur, Belgium (e-mail: laurent.schumacher@iee.org).

B. Raghoehtaman is with the Nokia Research Center, Dallas, TX 75039 USA (e-mail: balaji.raghoehtaman@nokia.com).

Digital Object Identifier 10.1109/TWC.2005.850275

¹In this paper, the AS is defined as the second central moment of the observed PAS.

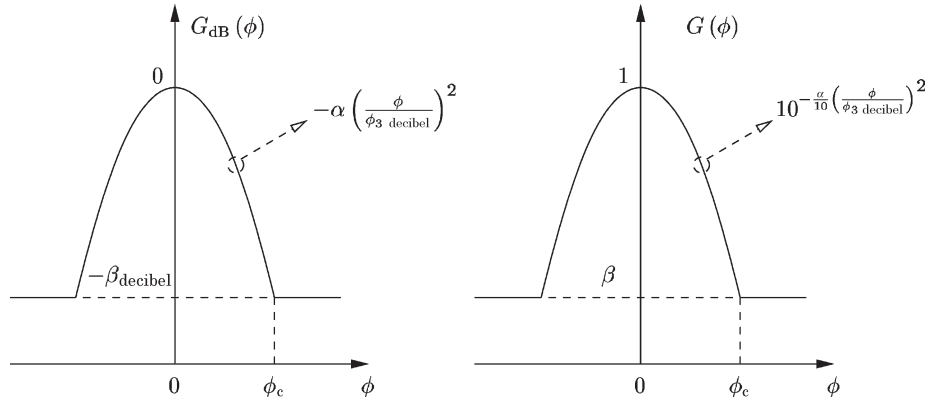


Fig. 1. Radiation pattern defined in [2].

where ϕ stands for the azimuth, α for a constant (set to 12 in [2]), $\phi_{3\text{ dB}}$ for the 3-dB beamwidth (in degrees), and β_{dB} for the maximum attenuation (in decibel). It combines a parabolic shape centered on the pointing azimuth and a constant floor. The power gain in linear scale can be derived from (1) with the help of $G(\phi) = 10^{G_{\text{dB}}(\phi)/10}$ and $\beta = 10^{-\beta_{\text{dB}}/10}$, leading to the drawing of Fig. 1. Based on the definition of the radiation pattern, the azimuth ϕ_c for which the parabolic shape crosses the constant value is derived from

$$-\alpha \left(\frac{\phi_c}{\phi_{3\text{ dB}}} \right)^2 = -\beta_{\text{dB}} \Rightarrow \phi_c = \phi_{3\text{ dB}} \sqrt{\frac{\beta_{\text{dB}}}{\alpha}} \quad (2)$$

as illustrated in Fig. 1.

B. Multimodal Laplacian PAS

The PAS of an impinging signal $s(t, \phi)$ is defined as

$$\text{PAS}(\phi) = \mathbb{E}_{\phi|\phi} [|s(t, \phi)|^2] \quad (3)$$

where $\mathbb{E}[\cdot]$ is the expectation operator. In order to be used as a probability density function (pdf), the PAS has to satisfy the condition

$$\int_{-\pi}^{\pi} \text{PAS}(\phi) d\phi = 1. \quad (4)$$

In the following, a particular type of PAS, namely, a multimodal truncated Laplacian PAS, is considered. The notion of a “multimodal” PAS was first introduced in [12]. Each mode corresponds to a resolvable cluster of waves whose spatial distribution can be modeled by a specific PAS of Laplacian type in the present case. “Truncated” means here that each mode is only defined within a limited interval $[\bar{\phi}_k - \Delta_k, \bar{\phi}_k + \Delta_k]$ of size $2\Delta_k$ centered on the angle of arrival (AoA) $\bar{\phi}_k$. The expression of a multimodal Laplacian PAS with N_c modes is then given by

$$\text{PAS}(\phi) = \sum_{k=1}^{N_c} \frac{Q_k}{\sqrt{2\sigma_k^2}} \exp \left[-\frac{\sqrt{2}|\phi - \bar{\phi}_k|}{\sigma_k} \right] \times w(\phi, \bar{\phi}_k - \Delta_k, \bar{\phi}_k + \Delta_k)$$

$$\text{where } w(\phi, a, b) = \begin{cases} 1, & \text{if } a < \phi < b \\ 0, & \text{otherwise} \end{cases} \quad (5)$$

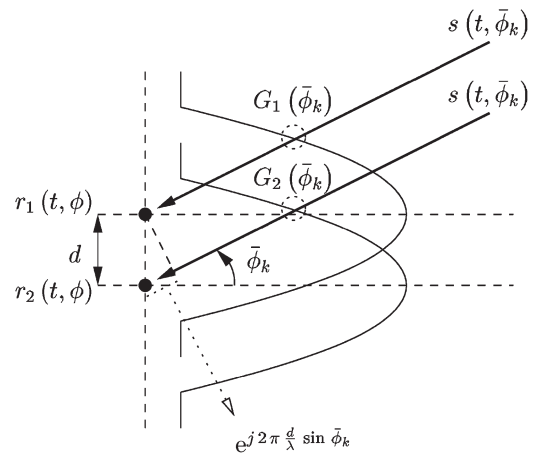


Fig. 2. Far-field signal impinging on two directive antenna elements.

where σ_k is the standard deviation of the Laplacian distribution and the normalization coefficients Q_k are computed so as to fulfill condition (4), leading to

$$\sum_{k=1}^{N_c} Q_k \left[1 - \exp \left(-\frac{\sqrt{2}\Delta_k}{\sigma_k} \right) \right] = 1. \quad (6)$$

III. CLOSED-FORM EXPRESSION FOR THE CORRELATION COEFFICIENT

Let us assume that the signal $s(t, \phi)$ impinges in far-field conditions on two antenna elements spaced by a distance d , each exhibiting a radiation pattern characterized by a power gain $G_i(\phi)$ where $i \in \{1, 2\}$. This scenario is depicted in Fig. 2. Note that this figure is slightly restrictive since both elements exhibit the same radiation pattern. This is a condition to be fulfilled in correlation-based multiple-input multiple-output (MIMO) stochastic channel models relying on the Kronecker product assumption [15]. Such models assume that all antenna elements at a given end illuminate the same set of scatterers.

Let

$$r_i(t, \phi) = \sqrt{G_i(\phi)} s(t, \phi) e^{j2\pi[f_c + (i-1)\frac{d}{\lambda} \sin \phi]} \quad (7)$$

denote the signal received at the i th antenna. f_c stands for the carrier frequency. The correlation coefficient between $r_1(t, \phi)$

and $r_2(t, \phi)$ can then be written as those in (8)–(11) shown at the bottom of the page, assuming that $s(t, \phi)$ is zero mean in any azimuth ϕ .

As already explained above, correlation-based MIMO channel models relying on the Kronecker product of correlation matrices defined independently at the transmitter and receiver require that all the antenna elements exhibit the same radiation pattern, i.e., $G_1(\phi) = G_2(\phi) = G(\phi)$. Using this property, we can rewrite ρ_{12} in (11) as

$$\rho_{12} = \frac{\int_{-\pi}^{\pi} e^{-j2\pi \frac{d}{\lambda} \sin \phi} \text{PAS}(\phi) G(\phi) d\phi}{\int_{-\pi}^{\pi} \text{PAS}(\phi) G(\phi) d\phi} \quad (12)$$

$$= \frac{\int_{-\pi}^{\pi} [\cos(D \sin \phi) - j \sin(D \sin \phi)] \text{PAS}(\phi) G(\phi) d\phi}{\int_{-\pi}^{\pi} \text{PAS}(\phi) G(\phi) d\phi} \quad (13)$$

$$= J_0(D) + 2 \sum_{m=1}^{+\infty} J_{2m}(D) \frac{\int_{-\pi}^{\pi} \cos(2m\phi) \text{PAS}(\phi) G(\phi) d\phi}{\int_{-\pi}^{\pi} \text{PAS}(\phi) G(\phi) d\phi} - 2j \sum_{m=0}^{\infty} J_{2m+1}(D) \frac{\int_{-\pi}^{\pi} \sin[(2m+1)\phi] \text{PAS}(\phi) G(\phi) d\phi}{\int_{-\pi}^{\pi} \text{PAS}(\phi) G(\phi) d\phi} \quad (14)$$

where $D = 2\pi(d/\lambda)$ stands for the normalized spacing between antenna elements, and the complex shift has been expanded with the help of Bessel functions of the first kind and of integer order [16].

The solution of (14) requires the evaluation of many integrals. The integrals are all of the form

$$\int_{-\pi}^{\pi} f(\phi) \text{PAS}(\phi) G(\phi) d\phi \quad (15)$$

where $f(\phi) \in \{1, \cos(2m\phi), \sin[(2m+1)\phi]\}$. Using (5), (15) becomes (16)–(18) found at the bottom of the next page.

In (18), in both integrals on the right-hand side, $f(\phi)$ can take three expressions. Furthermore, one should be aware that $G(\phi)$ is either a constant value or a parabolic function. Thus, there are 12 different forms of integrals to be evaluated: two half modes times three expressions of $f(\phi)$ times two expressions of $G(\phi)$. The closed-form expressions for all 12 are given in the Appendix. They can be grouped into three main categories, depending on the expression of $f(\phi)$. Within a given category, the closed-form expression of the indefinite integral to be used in (18) depends on the subsequent expansion of the absolute value $|\phi - \bar{\phi}_k|$ and of the gain $G(\phi)$. The actual expansion to be applied is determined by the relative positions of $\bar{\phi}_k$, $\bar{\phi}_k \pm \Delta_k$, and $\pm\phi_c$. For each mode of the PAS, three different situations, illustrated in Fig. 3, can be identified.

- 1) The mode is completely out of the scope of the parabolic part of the radiation pattern, either on the left-hand side ($\bar{\phi}_k + \Delta_k < -\phi_c$) or on the right-hand side ($\phi_c < \bar{\phi}_k - \Delta_k$).
- 2) Only half of the mode is impacted by the parabolic part of the radiation pattern, either on the left-hand side ($\bar{\phi}_k < -\phi_c < \bar{\phi}_k + \Delta_k$) or on the right-hand side ($\bar{\phi}_k - \Delta_k < \phi_c < \bar{\phi}_k$).
- 3) Both halves of the mode are impacted by the parabolic part of the radiation pattern.

Using the generic notation $FGH(A, B)$ to represent any of the four integrals of one category, where F stands for the expression of $f(\phi)$ ($F = F_O$ for $f(\phi) = 1$, $F = F_C$ for

$$\rho_{12} = \frac{\mathbf{E}_{t,\phi} [r_1(t, \phi) r_2^*(t, \phi)] - \mathbf{E}_{t,\phi} [r_1(t, \phi)] \mathbf{E}_{t,\phi} [r_2^*(t, \phi)]}{\sqrt{\mathbf{E}_{t,\phi} [|r_1(t, \phi)|^2]} \sqrt{\mathbf{E}_{t,\phi} [|r_2(t, \phi)|^2]}} \quad (8)$$

$$= \frac{\mathbf{E}_{t,\phi} [|s(t, \phi)|^2 \sqrt{G_1(\phi) G_2(\phi)} e^{-j2\pi \frac{d}{\lambda} \sin \phi}] - \mathbf{E}_{t,\phi} [s(t, \phi) \sqrt{G_1(\phi)}] \mathbf{E}_{t,\phi} [s(t, \phi) \sqrt{G_2(\phi)} e^{-j2\pi \frac{d}{\lambda} \sin \phi}]}{\sqrt{\mathbf{E}_{t,\phi} [|s(t, \phi) \sqrt{G_1(\phi)} |^2]} \sqrt{\mathbf{E}_{t,\phi} [|s(t, \phi) \sqrt{G_2(\phi)} |^2]}} \quad (9)$$

$$= \frac{\mathbf{E}_{\phi} \left\{ \mathbf{E}_{t|\phi} [|s(t, \phi)|^2] \sqrt{G_1(\phi) G_2(\phi)} e^{-j2\pi \frac{d}{\lambda} \sin \phi} \right\} - \mathbf{E}_{\phi} \left\{ \mathbf{E}_{t|\phi} [s(t, \phi) \sqrt{G_1(\phi)}] \mathbf{E}_{t|\phi} [s(t, \phi) \sqrt{G_2(\phi)}] \right\}}{\sqrt{\mathbf{E}_{\phi} \left\{ \mathbf{E}_{t|\phi} [|s(t, \phi)|^2] G_1(\phi) \right\}}} \sqrt{\mathbf{E}_{\phi} \left\{ \mathbf{E}_{t|\phi} [|s(t, \phi)|^2] G_2(\phi) \right\}} \quad (10)$$

$$= \frac{\int_{-\pi}^{\pi} e^{-j2\pi \frac{d}{\lambda} \sin \phi} \text{PAS}(\phi) \sqrt{G_1(\phi) G_2(\phi)} d\phi}{\sqrt{\int_{-\pi}^{\pi} \text{PAS}(\phi) G_1(\phi) d\phi} \sqrt{\int_{-\pi}^{\pi} \text{PAS}(\phi) G_2(\phi) d\phi}} \quad (11)$$

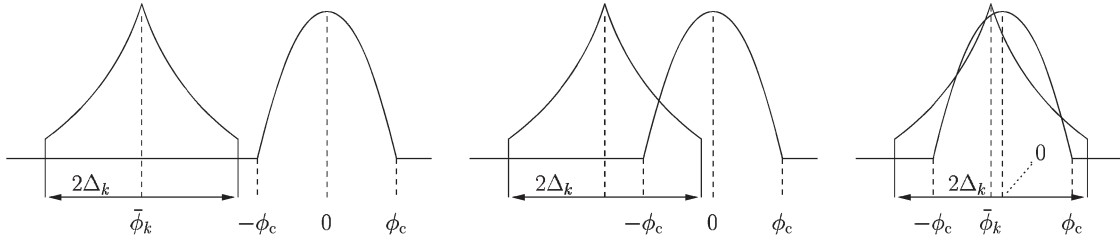


Fig. 3. Three situations of interaction between the PAS and the directive radiation pattern.

$f(\phi) = \cos(2m\phi)$, and $F = F_S$ for $f(\phi) = \sin[(2m+1)\phi]$, G stands for the radiation pattern ($G = G_C$ for the constant part and $G = G_P$ for the parabolic part), H for the half mode of the Laplacian PAS ($H = H_L$ for $\phi < \bar{\phi}_k$ and $H = H_R$ for $\phi > \bar{\phi}_k$), A for the lower integration limit, and B for the upper one, each integral of (18) can be written synthetically as that shown in (19) at the bottom of the next page.

IV. APPROXIMATION FOR SMALL ASS

Based on the relations (14), (18), and (19) and the indefinite integrals given in the Appendix, the value of the correlation coefficient can be computed. However, significant differences between the computed value and the numerical solution are observed for small ASSs. These discrepancies were traced to numerical problems with the evaluation of some expressions in the closed-form solution. Specifically, the imposition of definite integral limits on equations (36), (38), (44), and (46) given in the Appendix leads to expressions of the form

$$T \propto \exp\left[\frac{(a+jc)^2}{4b}\right] \left[\operatorname{erf}\left(\sqrt{b}\phi_2 \pm \frac{a+jc}{2\sqrt{b}}\right) - \operatorname{erf}\left(\sqrt{b}\phi_1 \pm \frac{a+jc}{2\sqrt{b}}\right) \right] \quad (20)$$

where $a \propto \sigma_k^{-1}$, b is a real constant, $c \propto m$, and ϕ_1, ϕ_2 represent the limits of the integral. The above expression can be written in the form $\chi(\xi_2 - \xi_1)$. For small ASSs, $|a+jc| \gg b$.

As a result, $\chi = \exp[(a+jc)^2/4b] \rightarrow \infty$ and $(\xi_2 - \xi_1) \rightarrow 0$. This computation of a quantity of the form $(\infty \times 0)$ leads to numerical instability.

To avoid this numerical problem, it makes sense, for small ASSs, to substitute the parabolic expression of the radiation pattern by a flat pattern whose gain is given by the value of the radiation pattern at $\phi = \bar{\phi}_k$. Mathematically, this leads to substituting the integrals in (18) by

$$\int_{\bar{\phi}_k - \Delta_k}^{\bar{\phi}_k + \Delta_k} f(\phi) \exp\left[-\frac{\sqrt{2}|\phi - \bar{\phi}_k|}{\sigma_k}\right] G(\phi) d\phi \approx \exp(-\gamma \bar{\phi}_k^2) \int_{\bar{\phi}_k - \Delta_k}^{\bar{\phi}_k + \Delta_k} f(\phi) \exp\left[-\frac{\sqrt{2}|\phi - \bar{\phi}_k|}{\sigma_k}\right] d\phi. \quad (21)$$

This approximation will be applied in the following whenever $\sigma_k \leq 5^\circ$.

V. VALIDATION

In order to validate the analytical developments presented in the previous sections and given in the Appendix, the closed-form expression for the correlation coefficient has been computed and the obtained value has been compared against the outcome of the numerical integration of the corresponding integrand. These comparisons are shown in Figs. 4–6. The first two

$$\int_{-\pi}^{\pi} f(\phi) \text{PAS}(\phi) G(\phi) d\phi = \int_{-\pi}^{\pi} f(\phi) \left\{ \sum_{k=1}^{N_c} \frac{Q_k}{\sqrt{2\sigma_k^2}} \exp\left[-\frac{\sqrt{2}|\phi - \bar{\phi}_k|}{\sigma_k}\right] w(\phi, \bar{\phi}_k - \Delta_k, \bar{\phi}_k + \Delta_k) \right\} G(\phi) d\phi \quad (16)$$

$$= \sum_{k=1}^{N_c} \frac{Q_k}{\sqrt{2\sigma_k^2}} \int_{\bar{\phi}_k - \Delta_k}^{\bar{\phi}_k + \Delta_k} f(\phi) \exp\left[-\frac{\sqrt{2}|\phi - \bar{\phi}_k|}{\sigma_k}\right] G(\phi) d\phi \quad (17)$$

$$= \sum_{k=1}^{N_c} \frac{Q_k}{\sqrt{2\sigma_k^2}} \left\{ \int_{\bar{\phi}_k - \Delta_k}^{\bar{\phi}_k} f(\phi) \exp\left[-\frac{\sqrt{2}(\bar{\phi}_k - \phi)}{\sigma_k}\right] G(\phi) d\phi + \int_{\bar{\phi}_k}^{\bar{\phi}_k + \Delta_k} f(\phi) \exp\left[-\frac{\sqrt{2}(\phi - \bar{\phi}_k)}{\sigma_k}\right] G(\phi) d\phi \right\} \quad (18)$$

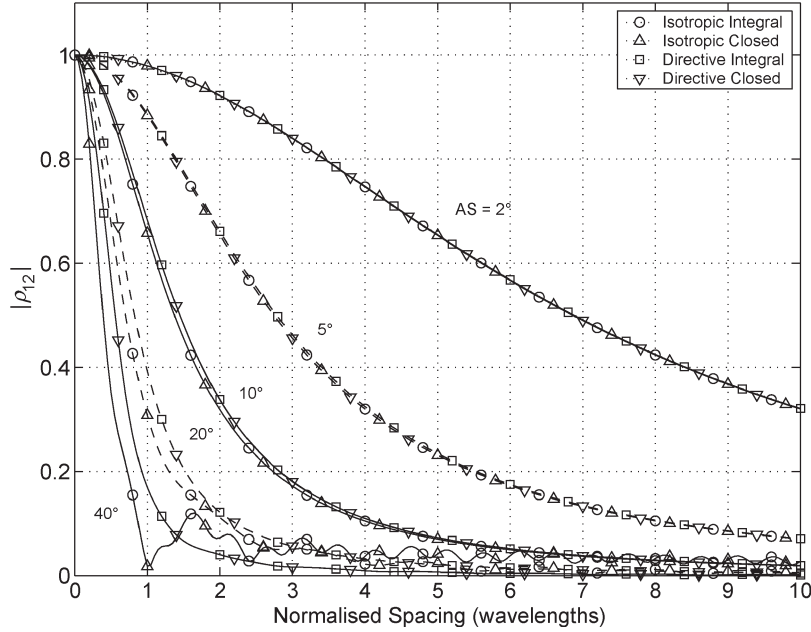


Fig. 4. Correlation coefficient of two antenna elements impinged by a monomodal truncated Laplacian PAS under an angle of incidence of 20° .

figures, Figs. 4 and 5, focus on monomodal Laplacian power azimuth spectra. The absolute value of the correlation coefficient is shown as a function of D , the normalized spacing between two antenna elements. By setting the parameters β_{dB} and $\phi_{3\text{ dB}}$ to different values, two scenarios have been considered: an omnidirectional scenario ($\beta_{\text{dB}} = 0$, $\phi_{3\text{ dB}}$ not meaningful) and a directive one as defined in [2] ($\beta_{\text{dB}} = 20$ and $\phi_{3\text{ dB}} = 70^\circ$). The comparison between the closed-form expression and the numerical integration has been performed for two AoAs, 20° (Fig. 4) and 50° (Fig. 5). Finally, for each AoA, different ASs (2° , 5° , 10° , 20° , and 40°) have been considered. Δ_k has been set to 180° .

First of all, a quasi-perfect match is acknowledged between the computed correlation values and the outcome of the numerical integration. The approximation for small ASs delivers reliable results but for large AoAs (Fig. 5) a small discrepancy is noticed between the closed-form computation and the numerical integration in the directive scenario. The computed value is then closer to the computed value in the omnidirectional scenario than to the numerical integration in the directive scenario. This can indicate that the limits of the validity of the approximation (21) have been reached. It should however be noted that the numerical integrations in omnidirectional and directive scenarios are very close. Nevertheless, in most cases,

$$\int_{\bar{\phi}_k - \Delta_k}^{\bar{\phi}_k + \Delta_k} f(\phi) \exp \left[-\frac{\sqrt{2}|\phi - \bar{\phi}_k|}{\sigma_k} \right] G(\phi) d\phi$$

$$= \begin{cases} FG_C H_L(\bar{\phi}_k - \Delta_k, \bar{\phi}_k) + FG_C H_R(\bar{\phi}_k, \bar{\phi}_k + \Delta_k), & \text{if } \bar{\phi}_k + \Delta_k < -\phi_c \\ FG_C H_L(\bar{\phi}_k - \Delta_k, \bar{\phi}_k) + FG_C H_R[\bar{\phi}_k, \max(\bar{\phi}_k, -\phi_c)] \\ \quad + FG_P H_R[\max(\bar{\phi}_k, -\phi_c), \min(\bar{\phi}_k + \Delta_k, \phi_c)] \\ \quad + FG_C H_R[\min(\bar{\phi}_k + \Delta_k, \phi_c), \bar{\phi}_k + \Delta_k], & \text{if } \bar{\phi}_k < -\phi_c < \bar{\phi}_k + \Delta_k \\ FG_C H_L[\bar{\phi}_k - \Delta_k, \max(\bar{\phi}_k - \Delta_k, -\phi_c)] \\ \quad + FG_P H_L[\max(\bar{\phi}_k - \Delta_k, -\phi_c), \bar{\phi}_k] \\ \quad + FG_P H_R[\bar{\phi}_k, \min(\bar{\phi}_k + \Delta_k, \phi_c)] \\ \quad + FG_C H_R[\min(\bar{\phi}_k + \Delta_k, \phi_c), \bar{\phi}_k + \Delta_k], & \text{if } -\phi_c < \bar{\phi}_k < \phi_c \\ FG_C H_L[\bar{\phi}_k - \Delta_k, \max(\bar{\phi}_k - \Delta_k, -\phi_c)] \\ \quad + FG_P H_L[\max(\bar{\phi}_k - \Delta_k, -\phi_c), \min(\bar{\phi}_k, \phi_c)] \\ \quad + FG_C H_L[\min(\bar{\phi}_k, \phi_c), \bar{\phi}_k] + FG_C H_R(\bar{\phi}_k, \bar{\phi}_k + \Delta_k), & \text{if } \bar{\phi}_k - \Delta_k < \phi_c < \bar{\phi}_k \\ FG_C H_L(\bar{\phi}_k - \Delta_k, \bar{\phi}_k) + FG_C H_R(\bar{\phi}_k, \bar{\phi}_k + \Delta_k), & \text{if } \phi_c < \bar{\phi}_k + \Delta_k. \end{cases} \quad (19)$$

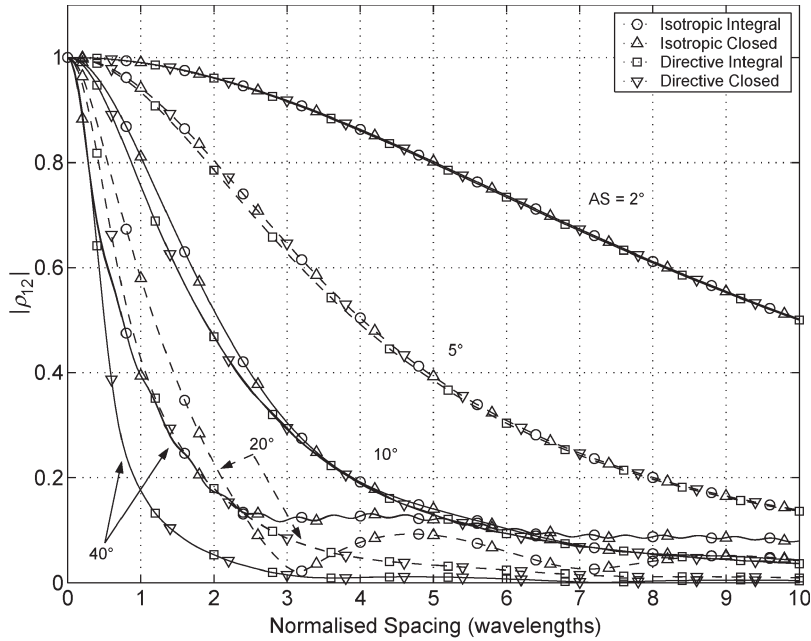


Fig. 5. Correlation coefficient of two antenna elements impinged by a monomodal truncated Laplacian PAS under an angle of incidence of 50° .

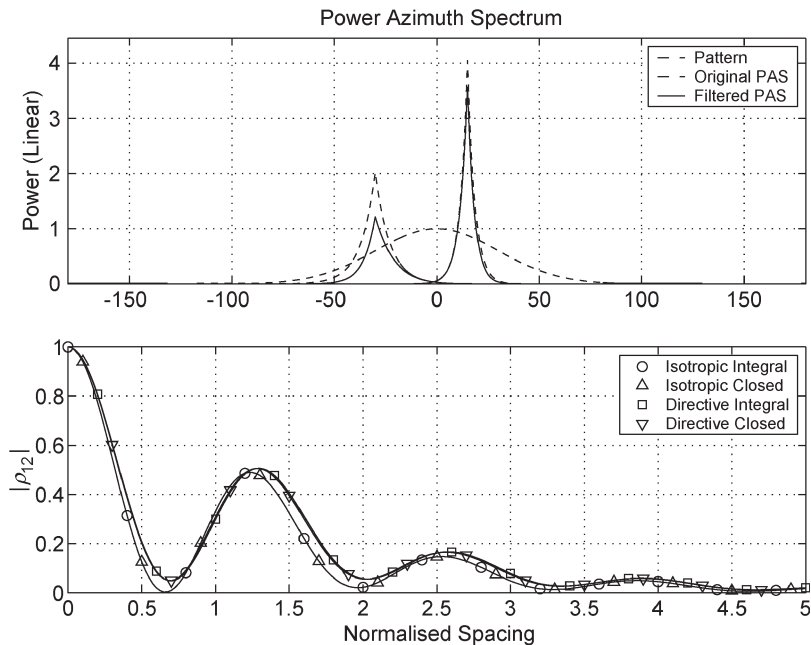


Fig. 6. Correlation coefficient of two antenna elements impinged by a bimodal truncated Laplacian PAS ($\text{AoA} = \{-30^\circ, 15^\circ\}$, $\text{AS} = \{10^\circ, 5^\circ\}$, $\Delta_\phi = 180^\circ$).

the computation of the closed-form expression delivers the correct value. The correctness of the computed values is further confirmed when looking at Table I, which compares computed correlation values to the ones presented in [2] for validation purposes. They agree within a small margin of 4%.

Having a closer look at the curves in Figs. 4 and 5, well-known trends can be observed, namely, that the correlation decreases for increasing normalized spacing, for increased AS and for decreasing AoA. It is also worthwhile to remark that for a given spacing and a given AS, the directive antennas tend to be slightly more correlated than the omnidirectional ones for small AoAs (Fig. 4), but that the opposite statement is to be made

for large AoAs (Fig. 5). With small AoAs, the PAS filtered by the directive radiation pattern seems sharper, hence the stronger correlation, whereas the same filtering effect under large AoAs attenuates the peak of the PAS with respect to its tails, as one can infer from Fig. 3.

A better understanding of the impact of the directive radiation pattern is built by considering the correlation coefficient shown in Fig. 6 for a bimodal scenario. The correlation coefficient increases due to the presence of the directive radiation pattern. Its impact on the impinging PAS is a reduction of the power of the outermost PAS, giving consequently more weight to the highly peaked PAS closer to the pointing azimuth of

TABLE I
REFERENCE AND COMPUTED CORRELATION COEFFICIENT VALUES FOR TEST CASES OF [2]

Spacing	AS (degree)	AoA (degree)	Complex			Real		
			Reference	Computed	Error (percent)	Reference	Computed	Error (percent)
.5λ	5	20	0.4743 + j 0.8448	0.4640 + j 0.8499	1.38	0.96884	0.96828	0.06
	2	50	-0.7367 + j 0.6725	-0.7390 + j 0.6699	3.44	0.99749	0.99752	0.01
4λ	5	20	-0.2144 + j 0.2408	-0.2203 + j 0.2318	3.25	0.32242	0.31976	0.82
	2	50	0.8025 + j 0.3158	0.7954 + j 0.3350	3.48	0.8624	0.86309	0.08
10λ	5	20	-0.0617 + j 0.034	-0.061884 + j 0.032678	2.09	0.070448	0.069982	0.66
	2	50	-0.2762 - j 0.4190	-0.26151 - j 0.42845	3.78	0.50184	0.50195	0.02

the pattern. Seen from the radiation pattern, the energy seems therefore to be more concentrated, thus a higher correlation coefficient.

VI. CONCLUSION

This document has presented the means to derive and compute the closed-form expression for the correlation coefficient of the signals received at two directive antennas exhibiting a widely used radiation pattern. The obtained expressions were validated against numerical integration. An upper bounded discrepancy of 4% was observed.

APPENDIX

This appendix presents the 12 indefinite integrals necessary to compute (14). They are grouped into three main categories, depending on the expression of $f(\phi)$. They will be represented with the generic notation FGH , where

- F stands for the expression of $f(\phi)$: $F = F_O$ for $f(\phi) = 1$, $F = F_C$ for $f(\phi) = \cos(2m\phi)$, and $F = F_S$ for $f(\phi) = \sin[(2m+1)\phi]$;
- G stands for the radiation pattern: $G = G_C$ for its constant part and $G = G_P$ for its parabolic part;
- H stands for the half mode of the PAS: $H = H_L$ for $\phi < \bar{\phi}_k$ and $H = H_R$ for $\phi > \bar{\phi}_k$.

A. First Category— $f(\phi) = 1$

$$F_O G_C H_L = \int \exp\left[-\frac{\sqrt{2}(\bar{\phi}_k - \phi)}{\sigma_k}\right] \beta d\phi \quad (22)$$

$$= \beta \frac{\sigma_k}{\sqrt{2}} \exp\left[\frac{\sqrt{2}(\phi - \bar{\phi}_k)}{\sigma_k}\right] \quad (23)$$

$$F_O G_C H_R = \int \exp\left[-\frac{\sqrt{2}(\phi - \bar{\phi}_k)}{\sigma_k}\right] \beta d\phi \quad (24)$$

$$= -\beta \frac{\sigma_k}{\sqrt{2}} \exp\left[\frac{\sqrt{2}(\bar{\phi}_k - \phi)}{\sigma_k}\right] \quad (25)$$

Setting $\gamma = (\alpha \ln 10)/(10 \phi_3^2 \text{ dB})$, the parabolic part writes

$$G_P(\phi) = 10^{-\frac{\alpha}{10} \left(\frac{\phi}{\phi_3 \text{ dB}}\right)^2} = \exp(-\gamma \phi^2). \quad (26)$$

Therefore

$$F_O G_P H_L = \int \exp\left[-\frac{\sqrt{2}(\bar{\phi}_k - \phi)}{\sigma_k}\right] \exp(-\gamma \phi^2) d\phi \quad (27)$$

$$= \frac{1}{2} \sqrt{\frac{\pi}{\gamma}} \exp\left(\frac{1 - 2\sqrt{2}\gamma\sigma_k\bar{\phi}_k}{2\gamma\sigma_k^2}\right) \times \text{erf}\left(\frac{\gamma\sqrt{2\sigma_k^2}\phi - 1}{\sqrt{2\gamma\sigma_k^2}}\right) \quad (28)$$

$$F_O G_P H_R = \int \exp\left[-\frac{\sqrt{2}(\phi - \bar{\phi}_k)}{\sigma_k}\right] \exp(-\gamma \phi^2) d\phi \quad (29)$$

$$= \frac{1}{2} \sqrt{\frac{\pi}{\gamma}} \exp\left(\frac{1 + 2\sqrt{2}\gamma\sigma_k\bar{\phi}_k}{2\gamma\sigma_k^2}\right) \times \text{erf}\left(\frac{\gamma\sqrt{2\sigma_k^2}\phi + 1}{\sqrt{2\gamma\sigma_k^2}}\right). \quad (30)$$

B. Second Category— $f(\phi) = \cos(2m\phi)$

With the help of [17, Relation 14.519, p. 85], one can derive

$$F_C G_C H_L = \int \cos(2m\phi) \exp\left[-\frac{\sqrt{2}(\bar{\phi}_k - \phi)}{\sigma_k}\right] \beta d\phi \quad (31)$$

$$= \beta \frac{\left(\frac{\sqrt{2}}{\sigma_k}\right) \cos(2m\phi) + 2m \sin(2m\phi)}{\left(\frac{\sqrt{2}}{\sigma_k}\right)^2 + 4m^2} \times \exp\left[\frac{\sqrt{2}(\phi - \bar{\phi}_k)}{\sigma_k}\right] \quad (32)$$

and

$$\begin{aligned}
 F_C G_C H_R &= \int \cos(2m\phi) \exp\left[-\frac{\sqrt{2}(\phi - \bar{\phi}_k)}{\sigma_k}\right] \beta d\phi \quad (33) \\
 &= \beta \frac{\left(-\frac{\sqrt{2}}{\sigma_k}\right) \cos(2m\phi) + 2m \sin(2m\phi)}{\left(\frac{\sqrt{2}}{\sigma_k}\right)^2 + 4m^2} \\
 &\quad \times \exp\left[\frac{\sqrt{2}(\bar{\phi}_k - \phi)}{\sigma_k}\right]. \quad (34)
 \end{aligned}$$

Additionally, using [18, p. 303], the two indefinite integrals that follow can be solved as

$$\begin{aligned}
 F_C G_P H_L &= \int \cos(2m\phi) \exp\left[-\frac{\sqrt{2}(\bar{\phi}_k - \phi)}{\sigma_k}\right] \exp(-\gamma\phi^2) d\phi \quad (35) \\
 &= \frac{1}{2} \sqrt{\frac{\pi}{\gamma}} \Re \{ \exp[X] \operatorname{erf}[Y] \} \\
 &\quad \text{where } X = \frac{(\sqrt{2} + j2m\sigma_k)^2 - 4\sqrt{2}\gamma\sigma_k\bar{\phi}_k}{4\gamma\sigma_k^2} \\
 &\quad \text{and } Y = \frac{2\gamma\sigma_k\phi - (\sqrt{2} + j2m\sigma_k)}{\sqrt{4\gamma\sigma_k^2}} \quad (36)
 \end{aligned}$$

and

$$\begin{aligned}
 F_C G_P H_R &= \int \cos(2m\phi) \exp\left[-\frac{\sqrt{2}(\phi - \bar{\phi}_k)}{\sigma_k}\right] \exp(-\gamma\phi^2) d\phi \quad (37) \\
 &= \frac{1}{2} \sqrt{\frac{\pi}{\gamma}} \Re \{ \exp[X] \operatorname{erf}[Y] \} \\
 &\quad \text{where } X = \frac{(\sqrt{2} + j2m\sigma_k)^2 + 4\sqrt{2}\gamma\sigma_k\bar{\phi}_k}{4\gamma\sigma_k^2} \\
 &\quad \text{and } Y = \frac{2\gamma\sigma_k\phi + (\sqrt{2} + j2m\sigma_k)}{\sqrt{4\gamma\sigma_k^2}} \quad (38)
 \end{aligned}$$

C. Third Category— $f(\phi) = \sin[(2m + 1)\phi]$

In a similar way to the approach adopted in the previous section and with the help of [17, Relation 14.518, p. 85] and [18, p. 303], the four indefinite integrals of this category are given by

$$\begin{aligned}
 F_S G_C H_L &= \int \sin[(2m + 1)\phi] \exp\left[-\frac{\sqrt{2}(\bar{\phi}_k - \phi)}{\sigma_k}\right] \beta d\phi \quad (39) \\
 &= \beta \frac{\left(\frac{\sqrt{2}}{\sigma_k}\right) \sin[(2m + 1)\phi] - (2m + 1) \cos[(2m + 1)\phi]}{\left(\frac{\sqrt{2}}{\sigma_k}\right)^2 + (2m + 1)^2} \\
 &\quad \times \exp\left[\frac{\sqrt{2}(\phi - \bar{\phi}_k)}{\sigma_k}\right] \quad (40)
 \end{aligned}$$

$$\begin{aligned}
 F_S G_C H_R &= \int \sin[(2m + 1)\phi] \exp\left[-\frac{\sqrt{2}(\phi - \bar{\phi}_k)}{\sigma_k}\right] \beta d\phi \quad (41) \\
 &= \beta \frac{\left(-\frac{\sqrt{2}}{\sigma_k}\right) \sin[(2m + 1)\phi] - (2m + 1) \cos[(2m + 1)\phi]}{\left(\frac{\sqrt{2}}{\sigma_k}\right)^2 + (2m + 1)^2} \\
 &\quad \times \exp\left[\frac{\sqrt{2}(\bar{\phi}_k - \phi)}{\sigma_k}\right] \quad (42)
 \end{aligned}$$

$$\begin{aligned}
 F_S G_P H_L &= \int \sin[(2m + 1)\phi] \exp\left[-\frac{\sqrt{2}(\bar{\phi}_k - \phi)}{\sigma_k}\right] \exp(-\gamma\phi^2) d\phi \quad (43) \\
 &= \frac{1}{2} \sqrt{\frac{\pi}{\gamma}} \Im \{ \exp(X) \operatorname{erf}(Y) \} \\
 &\quad \text{where } X = \frac{[\sqrt{2} + j(2m + 1)\sigma_k]^2 - 4\sqrt{2}\gamma\sigma_k\bar{\phi}_k}{4\gamma\sigma_k^2} \\
 &\quad \text{and } Y = \frac{2\gamma\sigma_k\phi - [\sqrt{2} + j(2m + 1)\sigma_k]}{\sqrt{4\gamma\sigma_k^2}} \quad (44)
 \end{aligned}$$

$$\begin{aligned}
 F_S G_P H_R &= \int \sin[(2m + 1)\phi] \exp\left[-\frac{\sqrt{2}(\phi - \bar{\phi}_k)}{\sigma_k}\right] \exp(-\gamma\phi^2) d\phi \quad (45) \\
 &= \frac{1}{2} \sqrt{\frac{\pi}{\gamma}} \Im \{ \exp(X) \operatorname{erf}(Y) \} \\
 &\quad \text{where } X = \frac{[\sqrt{2} - j(2m + 1)\sigma_k]^2 + 4\sqrt{2}\gamma\sigma_k\bar{\phi}_k}{4\gamma\sigma_k^2} \\
 &\quad \text{and } Y = \frac{2\gamma\sigma_k\phi + [\sqrt{2} - j(2m + 1)\sigma_k]}{\sqrt{4\gamma\sigma_k^2}}. \quad (46)
 \end{aligned}$$

ACKNOWLEDGMENT

The authors would like to thank the anonymous reviewers for their thorough reading and valuable comments.

REFERENCES

- [1] 3GPP2 TSG-C WG3 spatial channel model AHG, "1 × EV-DV spatial channel model evaluation methodology," Tech. Rep., Mar. 2002.
- [2] SCM Editors, "Spatial channel model text description—v4.2b," Tech. Rep. 3GPP-3GPP2 SCM-132, Apr. 2003.
- [3] F. Adachi, M. Feeny, A. Williamson, and J. Parsons, "Cross-correlation between the envelopes of 900 MHz signals received at a mobile radio base station site," *IEE Proc. F*, vol. 133, no. 6, pp. 506–512, Oct. 1986.
- [4] P. S. H. Leather and J. D. Parsons, "Handheld antenna diversity experiments at 450 MHz," in *IEE Colloq. Multipath Countermeasures*, London, U.K., 1996, pp. 4/1–4/6.

- [5] W. Lee, "Effects on correlation between two mobile radio base-station antennas," *IEEE Trans. Commun.*, vol. 21, no. 11, pp. 1214–1224, Nov. 1973.
- [6] J. Fuhl, A. F. Molisch, and E. Bonek, "Unified channel model for mobile radio systems with smart antennas," *IEEE Proc. Radar, Sonar, Navig.*, vol. 145, no. 1, pp. 32–41, Feb. 1998.
- [7] J. Salz and J. Winters, "Effect of fading correlation on adaptive arrays in digital mobile radio," *IEEE Trans. Veh. Technol.*, vol. 43, no. 4, pp. 1049–1057, Nov. 1994.
- [8] K. I. Pedersen, P. E. Mogensen, and B. H. Fleury, "Spatial channel characteristics in outdoor environments and their impact on BS antenna system performance," in *Proc. IEEE Vehicular Technology Conf. (VTC) 1998*, Ottawa, Canada, vol. 2, pp. 719–723.
- [9] G. D. Durgin and T. S. Rappaport, "Effects of multipath angular spread on the spatial cross-correlation of received voltage envelopes," in *Proc. IEEE Vehicular Technology Conf. (VTC'99)*, Houston, TX, pp. 996–1000.
- [10] M. Stege, J. Jelitto, M. Bronzel, and G. Fettweis, "A multiple-input multiple-output channel model for simulation of TX- and RX-diversity wireless systems," in *Proc. IEEE Vehicular Technology Conf. (VTC) 2000 Fall*, Boston, MA, vol. 2, pp. 833–839.
- [11] K. I. Pedersen, P. E. Mogensen, and B. H. Fleury, "A stochastic model of the temporal and azimuthal dispersion seen at the base station in outdoor propagation environments," *IEEE Trans. Veh. Technol.*, vol. 49, no. 2, pp. 437–447, Mar. 2000.
- [12] R. M. Buehrer, "The impact of angular energy distribution on spatial correlation," in *Proc. IEEE 56th Vehicular Technology Conf. (VTC) Fall 2002*, Vancouver, Canada, pp. 1173–1177.
- [13] Q. H. Spencer, B. D. Jeffs, M. A. Jensen, and A. L. Swindlehurst, "Modeling the statistical time and angle of arrival characteristics of an indoor multipath channel," *IEEE J. Sel. Areas Commun.*, vol. 18, no. 3, pp. 347–360, Mar. 2000.
- [14] A. Saleh and R. Valenzuela, "A statistical model for indoor multipath propagation," *IEEE J. Sel. Areas Commun.*, vol. 5, no. 2, pp. 128–137, Feb. 1987.
- [15] J. P. Kermaol, L. Schumacher, K. I. Pedersen, and P. E. Mogensen, "A stochastic MIMO radio channel model with experimental validation," *IEEE J. Sel. Areas Commun.*, vol. 20, no. 6, pp. 1211–1226, Aug. 2002.
- [16] G. N. Watson, *A Treatise on the Theory of Bessel Functions*, Cambridge Mathematical Library. Cambridge, U.K.: Cambridge Univ. Press, 1966.
- [17] M. R. Spiegel, *Formules et Tables de Mathématiques*. New York: McGraw-Hill, 1974.
- [18] *Handbook of Mathematical Functions with Formulas, Graphs and Mathematical Tables*, M. Abramowitz and I. A. Segun, Eds. New York: Dover, 1965.